HHS Public Access

Author manuscript

Science. Author manuscript; available in PMC 2018 May 17.

Published in final edited form as:

Science. 2017 October 13; 358(6360): . doi:10.1126/science.aao2602.

The Microanatomic Segregation of Selection by Apoptosis in the Germinal Center

Christian T. Mayer[1], **Anna Gazumyan**[1], **Ervin E. Kara**[1], **Alexander D. Gitlin**[1], **Jovana Golijanin**[1], **Charlotte Viant**[1], **Joy Pai**[1], **Thiago Y. Oliveira**[1], **Qiao Wang**[1], **Amelia Escolano**[1], **Max Medina-Ramirez**[2], **Rogier W. Sanders**[2,3], and **Michel C. Nussenzweig**[1,4,*]

[1]Laboratory of Molecular Immunology, The Rockefeller University, New York, NY 10065, USA [2]Department of Medical Microbiology, Academic Medical Center, University of Amsterdam, 1105 AZ Amsterdam, Netherlands [3]Department of Microbiology and Immunology, Weill Medical College of Cornell University, New York, NY 10065, USA [4]Howard Hughes Medical Institute (HHMI)

Abstract

B cells undergo rapid cell division and affinity maturation in anatomically distinct sites in lymphoid organs called germinal centers (GCs). Homeostasis is maintained in part by B-cell apoptosis. However, the precise contribution of apoptosis to GC biology and selection is not well defined. We developed apoptosis-indicator mice and used them to visualize, purify, and characterize dying GC B cells. Apoptosis is prevalent in the GC with up to half of all GC B cells dying every 6h. Moreover, programmed cell death is differentially regulated in the light zone (LZ) and the dark zone (DZ): LZ B cells die by default if they are not positively selected, whereas DZ cells die when their antigen receptors are damaged by activation-induced cytidine deaminase (AID).

Germinal centers (GCs) are divided into two anatomic compartments, the light zone (LZ) and the dark zone (DZ). B cells divide and undergo somatic hypermutation (SHM) in the DZ and are positively selected for affinity-enhancing mutations by interacting with T follicular helper (Tfh) cells in the LZ (1–3). Cell division is a dominant feature of the GC with rapid cell division rates of 4-6 h and up to 30% of cells in cycle at any time (1, 3, 4). Despite extensive cell division, the size of the GC compartment can be relatively constant for weeks or months (5). Equilibrium is attributed to a combination of cell death by apoptosis (negative selection), and emigration of memory and plasma cells from the GC. Emigration rates are estimated to be relatively low (< 0.1% for plasma cells (6) and < 2% for memory cells (7)). In contrast, cell loss by apoptosis is reported to be high (8, 9), but the precise rate and causes

*Correspondence to: nussen@rockefeller.edu.

Supplementary Materials:
Figures S1-S9
Table S1
Movies S1–S3

of apoptosis, its contribution to GC B-cell selection, and whether it is differentially regulated in the LZ and DZ of the GC has not been determined.

Negative selection in DZ and LZ

We used a monoclonal antibody against active caspase-3 (aCasp3) to identify apoptotic cells in the GCs of C57BL/6J mice immunized with either 4-hydroxy-3-nitrophenylacetyl (NP)-conjugated ovalbumin (NP-OVA), or an HIV-1 envelope antigen (BG505 SOSIP.v4.1-GT1.1 trimers, (GT1.1)). Whereas follicular (FO) B cells expressing aCasp3 were nearly absent, 3.6%-5.7% of GC B cells were aCasp3^{+} irrespective of the time of analysis or immunogen (Fig. 1A, B). Similarly, 3% of B cells in chronic GCs in Peyer's patches were aCasp3^{+} (fig. S1A, B). When compared to non-apoptotic cells, aCasp3^{+} GC B cells expressed slightly reduced levels of B220, Fas, CD19, CD86, and GL7, but comparable levels of activation-induced cytidine deaminase (AID), as indicated by an *AID*-GFP knock-in ((10), fig. S1C).

Analysis of apoptosis among DZ and LZ GC B cells revealed that 3.7%-5.7% of the DZ and 2.6%-5.6% of the LZ were aCasp3^{+} at all time points analyzed (Fig. 1C, D). Similar results were also obtained for Peyer's patch GC B cells (fig. S1E). Thus, the frequency of apoptotic GC B cells is relatively constant over time and nearly equivalent in LZ and DZ compartments.

The size of GCs in Peyer's patches is relatively constant over time in mice housed under specific pathogen-free conditions and thus, the number of dividing cells should equal the number of dying cells plus a small number that leave the GC to become memory B or plasma cells (6, 7, 11). To estimate the proportion of dividing cells in GCs, we performed kinetic labeling experiments with the nucleoside analog 5-ethynyl-2′-deoxyuridine (EdU), which is incorporated into DNA during the S phase. Approximately 50% of all Peyer's patch GC B cells were labeled by EdU in 5.3 h (Fig. 1E, F) suggesting that a large number of GC B cells are lost to cell death in this time.

Dynamics of dying GC B cells

To further characterize these events, we produced transgenic and knock-in mice that express an apoptosis reporter (INDIcator of Apoptosis, *Igκ^{INDIA}* and *Rosa26^{INDIA}*, fig. S2A and B). This reporter consists of an optimized Förster resonance energy transfer (FRET) pair, mNeonGreen and mRuby2, linked by a peptide containing an aCasp3-cleavage site (DEVDG, Fig. 2A). When aCasp3 cleaves the linker, mNeonGreen and mRuby2 should be separated, resulting in FRET loss and increased emission from mNeonGreen (Fig. 2A). Both *Igκ^{INDIA}* and *Rosa26^{INDIA}* B cells expressed the INDIA protein (fig. S2C). To validate the reporter, transgenic B cells were activated in vitro and induced to undergo apoptosis by incubation with staurosporine (12). Flow cytometry revealed two distinct populations based on the mNeonGreen/FRET ratio (termed "FRET loss"; Fig. 2B, left). Whereas FRET^{+} B cells were alive, FRET^{-} B cells were apoptotic as confirmed by aCasp3, TUNEL, or Annexin-V/DAPI staining (Fig. 2B and fig. S2D).

To examine the kinetics of activated B-cell death, we tracked FRET loss in real time in cultured *Igκ^{INDIA}* B cells (Fig. 2C and fig. S2E). On average, the first morphological signs

of apoptosis were observed within 12.5 min of FRET loss including cell shrinkage, bleb formation and changes in motility (Fig. 2C, D; fig. S2E and Movies S1–3). Secondary necrosis, as revealed by loss of membrane integrity and leakage (Fig. 2C, fig. S2E and Movies S1–3), was observed an average of 68 min after FRET loss (Fig. 2D). Similar results were obtained in vivo by tracking *Rosa26*^{INDIA} knock-in GC B-cell death using two-photon laser scanning microscopy (TPLSM). GC B-cell fragmentation occurred on average 20.6 min after FRET loss and was observed in both DZ and LZ compartments (Fig. 2E-G; Movies 1–3; fig. S3A and B). Thus, the apoptotic compartment in GCs turns over with rapid kinetics. At an apoptosis rate of 3% every 20.6 min (fig. S1A, B), 46% of GC B cells in Peyer's patches are estimated to be lost in 5.3 h, which agrees with our measurements made by EdU labeling (Fig. 1E, F). Thus, apoptosis is a major feature of the B-cell program in the GC.

Negative selection against damaged BCRs in the DZ

What causes the high level of GC B-cell apoptosis? GC B cells express AID, an enzyme that initiates class switch recombination (CSR) and SHM by creating base pair mismatches in DNA. The absence of AID in mice and humans is associated with enlarged GCs (13, 14) and reduced GC B-cell apoptosis as measured by aCasp3 (fig. S4A-E, and (15)). To determine whether AID differentially affects cell death in the two GC compartments, we stained AID-deficient DZ and LZ cells for aCasp3. The absence of AID was associated with a clear reduction in apoptosis primarily in the DZ (fig. S4F-H). Thus, AID activity is a key component of apoptosis in the DZ, and apoptosis appears to be differentially regulated in the DZ and LZ.

AID introduces random mutations in immunoglobulin (*Ig*) genes that can increase antibody affinity, but can also be deleterious. To determine how *Ig* mutation impacts apoptosis, we cloned antibodies from single FRET^{-} *Igκ*^{INDIA} GC B cells that had started undergoing apoptosis (Fig. 2H and fig. S5A). *Ig* heavy chain (*IgH*) and light chain (*Igκ* and *Igλ*) sequencing revealed that 94% and 83% of live NP-OVA- and GT1.1-elicited GC B cells carried intact B-cell receptors (BCRs), respectively (Fig. 2I, J; top). In contrast, only 68% and 59% of apoptotic NP-OVA- and GT1.1-elicited GC B cells carried BCR transcripts capable of producing *Ig* (Fig. 2I, J; top). The loss of BCR expression in the apoptotic compartment was confirmed by flow cytometry in NP-OVA-specific GCs and Peyer's patches, and was AID-dependent (fig. S5B, C). Apoptotic B cells with non-functional BCRs were highly enriched in the DZ over LZ: 43% and 58% of apoptotic DZ, and 9% and 14% in of apoptotic LZ GC B cells in NP-OVA- or GT1.1-immunized mice, respectively, carried non-productive *Ig* transcripts (Fig. 2I, J; bottom). This observation is consistent with reports that AID is expressed at higher levels and accesses DNA in proliferating DZ B cells (5, 16, 17). Although a majority of non-functional apoptotic DZ BCRs carried stop codons (63% and 69% in NP-OVA- and GT1.1-elicited GCs, respectively), a significant fraction (37% and 31%, respectively) was out-of-frame due to nucleotide insertions or deletions (fig. S5D, E). Thus, apoptotic DZ B cells are enriched for non-functional *Ig* transcripts as a consequence of AID activity. We hypothesize that the small number of apoptotic LZ GC B cells with non-functional BCRs derive from recent DZ emigrants in which a delay between aberrant *Ig*

gene mutation, loss of BCR expression and apoptosis has occurred, as has been reported for naïve B cells (18).

Characterization of monoclonal antibodies cloned from dying GC B cells

In addition to compromising the integrity of the BCR, SHM can also alter antibody affinity, produce autoreactive or polyreactive BCRs, or render *Ig* heavy- and light chains incompatible. To measure the contribution of each of these effects to GC B-cell apoptosis, we produced $IgH_{V1\text{-}72}$ Ig_{λ} α-NP antibodies cloned from GC B cells of NP-OVA-immunized $Ig\kappa^{INDIA}$ mice. The relative affinity to NP was measured by ELISA on NP_4- or NP_{25}-BSA. High-affinity antibodies bind better to NP_4-BSA than low-affinity antibodies, whereas both bind equally to NP_{25}-BSA (Fig. 3A; (19)). All but one of the 167 $IgH_{V1\text{-}72}$ Ig_{λ} GC-derived antibodies tested bound to NP_{25}-BSA (Fig. 3A, B). As might be expected from the observation that the DZ contains affinity-selected B cells, high-affinity antibodies were slightly overrepresented in the DZ over LZ compartment (60% and 46%, respectively; p = 0.089, Fig. 3C). This small increase in high-affinity reactivity in the DZ was confirmed by increased proportions of the affinity-enhancing W33L mutation in the DZ (fig. S6A, B). However, high- and low-affinity antibodies were equally distributed among live and apoptotic B cells in both GC compartments (Fig. 3A, B and fig. S6A). Thus, the observed differences in affinity between LZ and DZ are likely due to rapid transit of positively selected cells from the LZ to the DZ (1), as well as relatively longer dwell time of higher-affinity cells in the DZ (2), and not apoptosis.

To document autoreactivity, we performed HEp-2 ELISAs, which are used clinically to measure antibody binding to cytoplasmic and nuclear self-antigens. Only 8% of the $IgH_{V1\text{-}72}$ Ig_{λ} GC antibodies cloned from live B cells displayed autoreactivity (Fig. 3D and fig. S6C). Consistent with the possibility that autoreactive antibodies can be redeemed by continued SHM (20, 21), there were similar numbers of autoreactive cells in live and apoptotic compartments (Fig. 3D and fig. S6C). Thus, autoreactivity accounts for only a small fraction of the overall death in $IgH_{V1\text{-}72}$ Ig_{λ} NP-specific GC B cells and it is not strongly selected into the apoptotic compartment.

Memory B cells show increased polyreactivity relative to naïve B cells (22–25). In agreement with these observations, 21% of all live GC B cells were polyreactive, with a slightly higher abundance in DZ (27%) over LZ (16%) (Fig. 3E and fig. S6D). Moreover, polyreactive cells were equally represented in the live and apoptotic compartments. Therefore polyreactivity is neither positively nor negatively selected into the apoptotic compartment in the GC.

Nearly all *Igs* cloned from live GC B cells produced secreted antibodies in transient transfection experiments. In contrast, a significant fraction of the antibodies derived from apoptotic $IgH_{V1\text{-}72}$ Ig_{λ} GC B cells did not, despite functional *Ig* genes (Fig. 3F). This phenomenon was particularly prominent among apoptotic DZ cells, where approximately half of the clones did not produce secreted antibodies in transient transfection experiments. Despite the lack of secreted Ig, immunoblot analysis of transfected cell pellets showed normal levels of *IgH* and *Igλ* expression, suggesting that structural problems and/or

defective Ig pairing interfered with normal antibody secretion (fig. S7). Thus, a significant fraction of the apoptotic cells in NP-specific GCs express antibodies that are structurally compromised (28%), and this phenomenon is exclusive to DZ GC B cells. In summary, selection against SHMs that introduce nucleotide insertions or deletions, that produce stop codons, change the reading frame, or otherwise compromise $IgH_{V1\text{-}72}$ Ig_{λ} expression or stability account for 75% of all the apoptotic cells in the DZ of NP-specific GCs (Fig. 3G).

Isotype switching

AID initiates both SHM and CSR. To examine the role of CSR in regulating apoptosis independently of SHM, we analyzed Peyer's patches from $AID^{Cre/Cre}$ $IgH^{96K/96K}$ $Rosa26^{LSL\text{-}YFP}$ mice in which ~50% of GC B cells undergo Cre-mediated CSR to IgG1 in the absence of AID and SHM (fig. S8A, B; (22)). $IgG1^+$ GC B cells were enriched among apoptotic cells in both LZ and DZ. In contrast, IgM^+ cells were overrepresented in the live compartments (Fig. 3H and fig. S8B). Similar results were also obtained in Peyer's patches and in lymph nodes of NP-OVA-immunized AID-sufficient C57BL/6J mice (fig. S8C, D). Thus, $IgG1^+$ GC B cells are more prone to apoptosis than IgM-expressing cells irrespective of AID expression or SHM. This effect may be due to altered IgG1 BCR signaling as indicated by lower levels of *Nur77*-GFP induction in $IgG1^+$ when compared to IgM^+ GC B cells (22).

Apoptosis in the LZ due to absence of positive selection

Our data indicate that in contrast to the DZ, 80% of apoptotic LZ cells express intact, non-autoreactive BCRs whose antigen binding properties are similar to those found in the live compartment (Fig. 3A, B and G). The transition from the DZ to the LZ is associated with increased expression of genes that regulate apoptosis (1, 16). To examine the possibility that apoptosis may be the default fate for cells that are not positively selected in the LZ, we inhibited positive selection by blocking CD40/CD40L interaction with α-CD40L antibody (fig. S9A). Although GC size, and the number of positively selected cells undergoing proliferation decreased, the rate of LZ B-cell apoptosis remained similar (Fig. 4A and (26)). Absence of a measurable increase in apoptosis (26) in α-CD40L antibody-treated mice is consistent with the relatively small number of LZ B cells (5-10%) undergoing positive selection at any time (27).

To gain further insights into the mechanisms responsible for cell death in the LZ, we measured apoptosis in cells undergoing BCR signaling and positive selection using *Nur77*-GFP and *Myc*-GFP reporters, respectively (27–29). A fraction of LZ B cells expressed *Nur77*, but only a subset of these cells were protected from apoptosis (Fig. 4B, C and fig. S9B, C). In contrast, positive selection as indicated by *Myc*-GFP expression was associated with nearly complete protection from apoptosis (Fig. 4B, C and fig. S9B, C). Thus, positive selection as measured by *Myc* expression protects B cells from apoptosis, but BCR crosslinking alone, as measured by *Nur77*, appears to be insufficient.

Conclusions

We have investigated the causes of apoptosis, and their contribution to cell death in the LZ and DZ of GCs by combining a FRET-indicator of apoptosis, single-cell sorting, and antibody cloning. Only a small fraction of LZ GC B cells are positively selected to return to the DZ and undergo additional rounds of division, and this process is, in part, stochastic (1, 30). The element of chance appears to be introduced by random encounters between LZ B cells displaying high levels of pMHCII and cognate Tfh cells. Consistent with this notion, the apoptotic compartment in the LZ contained an arbitrary assortment of B cells including those with high-affinity BCRs (Fig. 3B). Thus, both low- and high-affinity B cells undergo apoptosis in the LZ, but high-affinity cells are more likely to become positively selected after they encounter cognate Tfh cells (1, 31, 32). In contrast, the DZ is the microanatomic site of antibody quality control by selection against deleterious mutations introduced by AID. B cells expressing *Ig*s damaged by SHM undergo apoptosis. The largest group of apoptotic B cells in the DZ arises by AID-mediated introduction of stop codons, insertions, or deletions into BCR genes (33). Thus, GC B cells resemble developing and naïve B cells in that they require BCR expression for survival (18, 34–36).

GC B cells are among the most rapidly dividing eukaryotic cells with cell cycle times as short as 4-6 h. Despite rapid cell division and limited export of memory and plasma cells, the size of the GC is relatively stable over periods of weeks. Our experiments indicate that GC homeostasis is maintained by high rates of cell death. Moreover, whereas positive selection occurs in the LZ, negative selection by apoptosis occurs in both GC zones but is differentially regulated in the LZ and DZ.

Methods

Generation of *Igκ*^{INDIA} transgenic mice and *Rosa26*^{INDIA} knock-in mice

INDIcator of Apoptosis (INDIA) cDNA was assembled from sequence-optimized N-terminally Myc-tagged mNeonGreen (37), an 18 amino acid linker bearing the aCasp3 cleavage site DEVD (SSSELSGDEVDGTSGSEF; (38)) and mRuby2 (39) by gBlocks Gene fragment synthesis (Integrated DNA Technologies), overlap PCR and standard cloning procedures.

To produce *Igk*^{INDIA} transgenic mice, INDIA was placed under transcriptional control of mouse *Igκ* regulatory elements as previously described (40, 41), with the modification that the entire open reading frame was placed after the non-coding *Vκ* exon followed by the *Igκ* polyadenylation signal. After sequence and vector integrity confirmation, the vector backbone was eliminated by NotI/MluI digestion, and the resulting 7.2kb fragment was injected into the pronuclei of fertilized C57BL/6J oocytes. Transgenic founder mice were identified by PCR (Table S1; annealing temperature 55°C) on tail DNA. The transgenic founder line *Igκ*^{INDIA} was selected and maintained by mating to C57BL/6J mice or by intercrossing. Genotyping was performed by flow cytometry on peripheral blood.

To generate *Rosa26*^{INDIA} knock-in mice, INDIA was cloned into the AscI site of the CTV targeting vector (42) that was a gift from Klaus Rajewsky (Addgene plasmid #15912). The

frt-flanked IRES-eGFP sequence was deleted by L-arabinose-inducible *Flp* recombineering in SW105 bacteria (43). In brief, *Flp* expression was induced by 0.09% (w/v) L-arabinose for 1 h at 32°C, followed by electroporation of 1 ng vector and growth on LB agar plates containing ampicillin over night at 32°C. Vector integrity and deletion of IRES-eGFP in the resulting clones were confirmed by restriction enzyme digestion and sequencing. CY2.4 albino C57BL/6J-Tyr$^{c\text{-}2J}$-derived ES cells were targeted with the modified CTV vector at the Gene Targeting Resource Center (The Rockefeller University) and homologous recombination was verified by Southern blot and PCR. Chimeric males obtained after blastocyst injection were crossed to B6(Cg)-Tyr$^{c\text{-}2J}$/J females. *Rosa26*$^{LSL\text{-}INDIA}$ mice exhibiting germline transmission were identified by PCR and crossed to B6.C-Tg(CMV-cre)1Cgn/J mice to induce germline deletion of the LSL cassette.

Rosa26$^{LSL\text{-}INDIA}$ CMV-cre^{+} offspring were crossed to C57BL/6J mice. The resulting CMV-cre^{-} offspring ubiquitously expressing INDIA were intercrossed to establish *Rosa26*^{INDIA} mice. Genotyping was performed by flow cytometry on peripheral blood.

Mice

B6.C-Tg(CMV-cre)1Cgn/J, B6(Cg)-Tyr$^{c\text{-}2J}$/J, B6.SJL and C57BL/6J mice were purchased from Jackson Laboratories. *AID*$^{Cre/Cre}$*IgH*$^{96K/96K}$*Rosa26*$^{LSL\text{-}YFP}$, *AID*$^{-/-}$, *AID*-GFP, *Nur77*-GFP, *Myc*-GFP and B1-8^{hi} mice were described previously (10, 13, 22, 28, 29, 44, 45). Bone marrow chimeras were generated as described (46). All animal experiments were approved by the Institutional Review Board and the IACUC at The Rockefeller University.

Immunizations and treatments

Primary GCs were elicited by immunizing mice of the indicated genotypes subcutaneously with 25 μl of PBS containing 12.5 μg of NP_{15}-OVA (Biosearch Technologies) or 4 μg of HIV envelope antigen (BG505 SOSIP.v4.1-GT1.1 trimers, (GT1.1); provided by Rogier W. Sanders, Weill Medical College of Cornell University, New York) precipitated in alum (Imject alum, ThermoFisher Scientific) at a 2:1 ratio. *Igκ*^{INDIA} mice were also immunized intraperitoneally with 100 μl of PBS containing 50 μg of NP_{15}-OVA precipitated in alum. For blocking CD40L/CD40 interactions, immunized mice were injected intravenously with 300 μg of α-CD40L (MR-1, Bio X Cell) or 300 μg of Armenian Hamster IgG (Bio X Cell). To estimate dynamic GC B-cell loss by apoptosis, mice were injected intraperitoneally with 1 mg of 5-ethynyl-2′-deoxyuridine (EdU; ThermoFisher Scientific) every 2 h for up to 10 h. For identifying GC B cells in S phase, mice were given a single intravenous pulse of 1 mg of EdU 1.0 h - 2.5 h prior to sacrifice. To elicit secondary GCs, mice were immunized intraperitoneally with 100 μl of PBS containing 50 μg of OVA (Grade V, Sigma) precipitated in alum. Two weeks later, mice received 5×10^6 B1-8^{hi} B cells intravenously ($\approx5\times10^5$ Igλ^{+} NP-specific B cells; 5% *Rosa26*^{INDIA}/95% *Rosa26*^{WT}) followed one day later by a subcutaneous boost with 25 μl of PBS containing 25 μg of NP_{15}-OVA (Biosearch Technologies). Follicular dendritic cells (FDC) were labeled by intravenous injection of 0.5-1.0 mg of polyclonal rabbit α-B-Phycoerythrin (α-B-PE, Rockland) 4 d after boost immunization, followed 1 d later by subcutaneous injection of 0.05 μg B-PE (Thermo Fisher Scientific).

B-cell isolation and culture

B cells were purified from spleens and subcutaneous lymph nodes as previously described (2). *Igκ*^{INDIA} B cells were stimulated for 4 d with 25 μg/ml of LPS (L-2630, Sigma) and 5 ng/ml of IL-4 (I1020, Sigma) in vitro as described (47). Activated B cells were harvested, washed and cultured at 2×10^6 cells/ml with LPS/IL-4-free media for 3 h in the presence of 1 μM staurosporine (1285, Tocris) to induce apoptosis. GC B cells were enriched from immunized *Igκ*^{INDIA} mice by incubating single-cell suspensions with 1.25 μg/ml of biotinylated α-IgD for 10 min on ice followed by incubation with α-Biotin- and mouse CD43 MicroBeads (Miltenyi Biotech). Cells were passed through a magnetized LS column (Miltenyi Biotec) and enriched GC B cells were collected in the flow-through.

Live imaging of cultured B cells

On day 4, LPS/IL-4-activated *Igκ*^{INDIA} B cells were washed and placed in a 35-mm μ-Dish (Ibidi). After the addition of 1 μM staurosporine, cells were imaged in an environmental chamber set to 37°C using a DeltaVision Inverted Olympus IX-71 Image Restoration Microscope (GE Healthcare) with an Insight SSI 7 color solid state illumination system and a 20× dry objective. Separate excitation and emission filter wheels were employed to collect data for mNeonGreen (488-nm excitation; 525/50 BP), FRET (488-nm excitation; 632/60 BP) and standard brightfield images for each time point. 512 × 512 pixel images were taken every 60 s for 3 h using Ultimate Focus and a Prior SYZ piezo stage for multiple point visiting. Images were processed and analyzed with ImageJ 1.48q (National Institutes of Health) and videos were generated at a frame rate of 10 fps.

Intravital imaging and image analysis

Intravital imaging of popliteal lymph nodes and image acquisition were essentially performed as described previously (31). Mice were anesthetized by the inhalation of 4% isofluorane in pure oxygen, placed on a stage warmer set to 37 °C and maintained on anesthesia by inhalation of 1.25% isofluorane in pure oxygen. Popliteal lymph nodes in shaved hind legs were exposed by microsurgery and animals were placed under the heated Olympus 25× 1.05 NA Plan objective of an Olympus BX61 upright microscope fitted with a Coherent Chameleon Vision II IR laser. The femtosecond-pulsed multiphoton laser was tuned to 900 nm. A filter cube containing a 690LP mirror followed by a 495LP mirror was used to split the emission to either 2 GaAsp detectors (with a 500-550-nm filter for mNeonGreen fluorescence and a 575-630-nm filter for FRET fluorescence) and a PMT detector (with a 460-500-nm filter for CFP/autofluorescence). Images were acquired every 30 s as 75-μm Z-stacks (5-μm steps) with 1.4× zoom and with 512 × 512 X-Y resolution. Imaris software (Bitplane) was used to process data. Collapsed Z-stacks were exported as TIFF series from Imaris and videos were generated in ImageJ (National Institutes of Health) at a frame rate of 7 fps. The colocalization tool in Imaris was used to detect B1-8^{hi} *Rosa26*^{INDIA} GC B cells that were mNeonGreen$^+$ and lacked CFP/autofluorescence. The surface tool in Imaris was used to track mNeonGreen$^+$ GC B cells and the mean fluorescence intensities of mNeonGreen and FRET channels over time. The FRET loss ratio was calculated by dividing mNeonGreen and FRET fluorescence.

Flow cytometry

Spleens and lymph nodes were collected in RPMI media containing 6% of serum on ice. Single-cell suspensions were obtained by forcing the tissue through a 70-μm cell strainer (BD Biosciences). All centrifugation steps were performed at 4°C and cells were otherwise handled on ice to minimize apoptosis. Erythrocytes were lysed with 1 ml of ACK lysing buffer (Gibco) for 3 min on ice. After incubation with 5 μg/ml of α-CD16/32 (rat mAb 2.4G2, Bio X Cell) for 20 min at 4 °C, biotinylated α-CXCR4 was incubated for 45 min at 4°C. Biotin and additional surface antigens were detected by staining for 30 min at 4 °C. The Fixation/Permeabilization Solution Kit (BD Biosciences) was used for intracellular staining. α-CD19 (rat mAb eBio1D3), α-CD38 (rat mAb 90), α-CD45R/B220 (rat mAb RA3-6B2) and α-IgM (rat mAb II/41) were from eBioscience. α-CD19 (rat mAb 6D5) and α-CD86 (rat mAb 6D5) were from Biolegend. α-aCasp3 (Alexa Fluor 647-conjugated; rabbit mAb C92-605), α-CXCR4 (rat mAb 2B11), α-Fas (hamster mAb Jo2), α-Igκ (rat mAb 187.1), α-Igλ$_{1-3}$ (rat mAb R26-46), α-IgG1 (rat mAb A85-1), streptavidin conjugated to V500, and α-T- and B-cell activation antigen (rat mAb GL7) were from BD Biosciences. Alexa Fluor 647-conjugated polyclonal rabbit IgG was from Cell signaling. EdU was detected with the Click-iT Plus EdU Alexa Fluor 488 Flow Cytometry Assay Kit (ThermoFisher Scientific). Alexa Fluor 647-conjugated Annexin-V and 5 × Annexin Binding Buffer for flow cytometry were from ThermoFisher Scientific. Annexin-V staining was performed for 15 min at room temperature (1:50 dilution) and DAPI (Sigma) was added at 0.04 μg/ml prior to acquisition. TUNEL staining was carried out with the Apo-BrdU Apoptosis Detection Kit and Alexa Fluor 647-conjugated α-BrdU (mouse mAb MoBU-1, both from ThermoFisher Scientific) according to the manufacturer's instructions.

Flow cytometry data were acquired on a BD Fortessa (BD Biosciences) and data were analyzed with Flowjo (Tristar). Intact cells and singlets were identified by their FSC/SSC profiles and in the case of *Igκ^{INDIA}* B cells additionally by mRuby2 expression (561-nm excitation; 582/15 BP). FO B cells were gated CD19^{+}CD38^{+}Fas^{-} and GC B cells were gated CD19^{+}CD38^{-}Fas^{+} and additionally GL7^{+} where indicated. Live and apoptotic fractions were discriminated by aCasp3 staining, or by mNeonGreen (488-nm excitation; 505LP and 530/30 BP) and FRET (488-nm excitation; 600LP and 610/20 BP) for *Igκ^{INDIA}* mice. FRET loss was derived as a separate parameter in Flowjo defined as the ratio of mNeonGreen and FRET fluorescence among intact mRuby2^{+} B cells. GC B-cell fractions were differentiated into LZ (CXCR4^{lo}CD86^{hi}) and DZ (CXCR4^{hi}CD86^{lo}) where indicated. Due to lower expression of CD86 in apoptotic compared to live GC B cells (see fig. S1), DZ and LZ were separately gated for live and apoptotic GC compartments. Apoptosis rates in DZ and LZ were calculated as: (% aCasp3^{+} of GC) × (% DZ or LZ of aCasp3^{+} GC)/(% DZ or LZ of total GC).

Cell sorting

Cell sorting was carried out on a FACS Aria II (BD Biosciences). For bulk sorting, cultured *Igκ^{INDIA}* B cells were washed and directly re-suspended in PBS containing 1% serum and 2 mM EDTA. For single-cell sorting, *Igκ^{INDIA}* GC B cells were identified as B220^{+}DUMP^{-}CD38^{-}Fas^{+} (DUMP = TCRβ/F4/80/Gr-1/NK1.1/CD11c). Intact cells and singlets were identified by their FSC/SSC profiles and by mRuby2 expression (561-nm excitation; 570LP,

585/15 BP). Live and apoptotic fractions were discriminated based on mNeonGreen (488-nm excitation; 505LP and 530/30 BP), FRET (488-nm excitation; 595LP and 610/20 BP) and B220 signals (Live: $FRET^{+}B220^{+}$; apoptotic: $FRET^{-}B220^{lo}$). Live and apoptotic GC B-cell fractions were further differentiated into LZ ($CXCR4^{lo}CD86^{hi}$) and DZ ($CXCR4^{hi}CD86^{lo}$). Single GC B cells of each compartment were sorted into 96-well PCR plates containing 4μl lysis buffer (48) and were either directly processed or stored at −80°C.

Single-cell cloning and recombinant antibody expression

Reverse transcription, nested PCR amplification, sequencing and ligation-independent cloning of *IgG1*, Ig*λ* and *Igκ* were as described (48, 49) with minor modifications. *IgM* sequences were amplified in the same reaction as *IgG1* by adding specific reverse primers (First PCR: 5′-AGGGGGCTCTCGCAGGAGACGAGG-3′; sequencing PCR: 5′-AGGGGGAAGACATTTGGGAAGGAC-3′). A specific forward primer (5′-CTAGTAGCAACTGCAACCGGTGTACATTCTCAGGTGCAGCTGCAGGAGTC-3′) was used to amplify and clone $IgH_{V1\text{-}72}$. Sequences were analyzed with IMGT/V-QUEST and IgBlast. Some *Ig* sequences were directly ordered from Genscript. The VDJ sequences of NP-specific antibodies B1-8, B1-8^{hi} and B1-8^{lo} (3C52) were previously described (45, 50, 51) and synthesized by Genscript. *Ig* sequences were cloned into human IgG1 and human Igλ expression vectors, and $IgH_{V1\text{-}72}$ Ig_{λ} monoclonal antibodies were expressed by transient transfection of HEK293-6E cells and purified with Protein G Sepharose 4 Fast Flow (GE Healthcare) as described (48). Some antibodies that appeared to be instable in PBS pH 7.0 were instead buffer exchanged into 20 mM acetic acid/sodium acetate buffer containing 9% sucrose (pH 5.2).

Immunoblot Analysis

Transfected HEK293-6E cell cultures were collected on day 7, centrifuged and the supernatant was harvested. The cell pellet was lysed (1% SDS, 10 mM EDTA, 50 mM Tris/HCl, pH 8) and sonicated for 10 min. Antibodies were analyzed in the matched supernatants and cell pellets by SDS-PAGE and immunoblot. HRP-conjugated goat α-human IgG (H+L) antibody (Jackson ImmunoResearch, cat# 109-036-088) was detected with HyGLO Quick Spray (Denville Scientific).

ELISAs

Autoreactivity against nuclear and cytoplasmic self-antigens was determined with QUANTA Lite ANA ELISA (Inova Diagnostics) as described (52). Polyreactivity against ssDNA, dsDNA, Keyhole limpet hemocyanin (KLH), human insulin and lipopolysaccharide (LPS) was determined as described (22). To measure NP binding, high-binding 96-well plates (Corning) were coated overnight with 50 μl of PBS containing 10 μg/ml of NP_4-BSA or NP_{25}-BSA (Biosearch Technologies). After washing with PBS containing 0.05% of Tween 20 (Sigma), wells were blocked with PBS containing 1% of BSA for 2 h at room temperature. Monoclonal antibodies were incubated at 4 μg/ml or 7 consecutive 1:4 dilutions in PBS for 2 h at room temperature. After washing, HRP-conjugated goat α-human IgG (Jackson ImmunoResearch) was added at 0.16 μg/ml for 1 h at room temperature. After additional washing, HRP was revealed with 1-Step ABTS Substrate Solution (ThermoFisher

Scientific). Absorbance was measured at 405 nm after incubation for 20 min at room temperature.

Statistical analyses

Statistical significance was determined with Graphpad Prism Version 6.0 using the tests indicated in each figure.

Supplementary Material

Refer to Web version on PubMed Central for supplementary material.

Acknowledgments

We thank Thomas Eisenreich for help with mouse colony management; Kai-Hui Yao for technical help; Kristie M. Gordon and Neena M. Thomas for cell sorting; Drs. John Moore, Davide Robbiani, Mila Jankovic, and all members of the Nussenzweig laboratory for discussion. We further thank Dr. Chingwen Yang, the Gene Targeting Resource Center, and Drs. Alison North and Kaye Thomas from the Bio-imaging Resource Center of The Rockefeller University with support by the Empire State Stem Cell Fund through NYSDOH Contract #C023046. Opinions expressed here are solely those of the author and do not necessarily reflect those of the Empire State Stem Cell Fund, the NYSDOH, or the State of NY. The data presented in this manuscript are tabulated in the main paper and in the supplementary materials. C.T.M. was supported by an EMBO long-term fellowship (ALTF 456-2014) and by the European Commission FP7 (Marie Curie Actions, EMBOCOFUND2012, GA-2012-600394). A.D.G. was supported by the NIH Medical Scientist Training Program grant T32GM07739 and the National Institute of Allergy and Infectious Diseases, NIH, grant F30-AI109903-03. M.C.N. is an HHMI investigator.

References and Notes

1. Victora GD, et al. Germinal center dynamics revealed by multiphoton microscopy with a photoactivatable fluorescent reporter. Cell. 2010; 143:592–605. [PubMed: 21074050]
2. Gitlin AD, Shulman Z, Nussenzweig MC. Clonal selection in the germinal centre by regulated proliferation and hypermutation. Nature. 2014; 509:637–640. [PubMed: 24805232]
3. Allen CD, Okada T, Tang HL, Cyster JG. Imaging of germinal center selection events during affinity maturation. Science. 2007; 315:528–531. [PubMed: 17185562]
4. Hauser AE, et al. Definition of germinal-center B cell migration in vivo reveals predominant intrazonal circulation patterns. Immunity. 2007; 26:655–667. [PubMed: 17509908]
5. Robbiani DF, et al. Plasmodium Infection Promotes Genomic Instability and AID-Dependent B Cell Lymphoma. Cell. 2015; 162:727–737. [PubMed: 26276629]
6. Fooksman DR, et al. Development and migration of plasma cells in the mouse lymph node. Immunity. 2010; 33:118–127. [PubMed: 20619695]
7. Laidlaw BJ, et al. The Eph-related tyrosine kinase ligand Ephrin-B1 marks germinal center and memory precursor B cells. J Exp Med. 2017; 214:639–649. [PubMed: 28143955]
8. Liu YJ, et al. Mechanism of antigen-driven selection in germinal centres. Nature. 1989; 342:929–931. [PubMed: 2594086]
9. Liu YJ, et al. Germinal center cells express bcl-2 protein after activation by signals which prevent their entry into apoptosis. Eur J Immunol. 1991; 21:1905–1910. [PubMed: 1868875]
10. Crouch EE, et al. Regulation of AID expression in the immune response. J Exp Med. 2007; 204:1145–1156. [PubMed: 17452520]
11. Butcher EC, et al. Surface phenotype of Peyer's patch germinal center cells: implications for the role of germinal centers in B cell differentiation. J Immunol. 1982; 129:2698–2707. [PubMed: 6982940]
12. Chae HJ, et al. Molecular mechanism of staurosporine-induced apoptosis in osteoblasts. Pharmacol Res. 2000; 42:373–381. [PubMed: 10987998]

13. Muramatsu M, et al. Class switch recombination and hypermutation require activation-induced cytidine deaminase (AID), a potential RNA editing enzyme. Cell. 2000; 102:553–563. [PubMed: 11007474]
14. Revy P, et al. Activation-induced cytidine deaminase (AID) deficiency causes the autosomal recessive form of the Hyper-IgM syndrome (HIGM2). Cell. 2000; 102:565–575. [PubMed: 11007475]
15. Zaheen A, et al. AID constrains germinal center size by rendering B cells susceptible to apoptosis. Blood. 2009; 114:547–554. [PubMed: 19478044]
16. Victora GD, et al. Identification of human germinal center light and dark zone cells and their relationship to human B-cell lymphomas. Blood. 2012; 120:2240–2248. [PubMed: 22740445]
17. Wang Q, et al. The cell cycle restricts activation-induced cytidine deaminase activity to early G1. J Exp Med. 2017; 214:49–58. [PubMed: 27998928]
18. Kraus M, Alimzhanov MB, Rajewsky N, Rajewsky K. Survival of resting mature B lymphocytes depends on BCR signaling via the Igalpha/beta heterodimer. Cell. 2004; 117:787–800. [PubMed: 15186779]
19. Takahashi Y, Dutta PR, Cerasoli DM, Kelsoe G. In situ studies of the primary immune response to (4-hydroxy-3-nitrophenyl)acetyl. V. Affinity maturation develops in two stages of clonal selection. J Exp Med. 1998; 187:885–895. [PubMed: 9500791]
20. Tan J, et al. A LAIR1 insertion generates broadly reactive antibodies against malaria variant antigens. Nature. 2016; 529:105–109. [PubMed: 26700814]
21. Reed JH, Jackson J, Christ D, Goodnow CC. Clonal redemption of autoantibodies by somatic hypermutation away from self-reactivity during human immunization. J Exp Med. 2016; 213:1255–1265. [PubMed: 27298445]
22. Gitlin AD, et al. Independent Roles of Switching and Hypermutation in the Development and Persistence of B Lymphocyte Memory. Immunity. 2016; 44:769–781. [PubMed: 26944202]
23. Tiller T, et al. Autoreactivity in human IgG+ memory B cells. Immunity. 2007; 26:205–213. [PubMed: 17306569]
24. Scheid JF, et al. Differential regulation of self-reactivity discriminates between IgG+ human circulating memory B cells and bone marrow plasma cells. Proc Natl Acad Sci U S A. 2011; 108:18044–18048. [PubMed: 22025722]
25. Mietzner B, et al. Autoreactive IgG memory antibodies in patients with systemic lupus erythematosus arise from nonreactive and polyreactive precursors. Proc Natl Acad Sci U S A. 2008; 105:9727–9732. [PubMed: 18621685]
26. Han S, Zheng B, Dal Porto J, Kelsoe G. In situ studies of the primary immune response to (4-hydroxy-3-nitrophenyl)acetyl. IV. Affinity-dependent, antigen-driven B cell apoptosis in germinal centers as a mechanism for maintaining self-tolerance. J Exp Med. 1995; 182:1635–1644. [PubMed: 7500008]
27. Dominguez-Sola D, et al. The proto-oncogene MYC is required for selection in the germinal center and cyclic reentry. Nat Immunol. 2012; 13:1083–1091. [PubMed: 23001145]
28. Huang CY, Bredemeyer AL, Walker LM, Bassing CH, Sleckman BP. Dynamic regulation of c-Myc proto-oncogene expression during lymphocyte development revealed by a GFP-c-Myc knock-in mouse. Eur J Immunol. 2008; 38:342–349. [PubMed: 18196519]
29. Mueller J, Matloubian M, Zikherman J. Cutting edge: An in vivo reporter reveals active B cell receptor signaling in the germinal center. J Immunol. 2015; 194:2993–2997. [PubMed: 25725108]
30. Tas JM, et al. Visualizing antibody affinity maturation in germinal centers. Science. 2016; 351:1048–1054. [PubMed: 26912368]
31. Shulman Z, et al. Dynamic signaling by T follicular helper cells during germinal center B cell selection. Science. 2014; 345:1058–1062. [PubMed: 25170154]
32. Shulman Z, et al. T follicular helper cell dynamics in germinal centers. Science. 2013; 341:673–677. [PubMed: 23887872]
33. Yeap LS, et al. Sequence-Intrinsic Mechanisms that Target AID Mutational Outcomes on Antibody Genes. Cell. 2015; 163:1124–1137. [PubMed: 26582132]
34. Lam KP, Kuhn R, Rajewsky K. In vivo ablation of surface immunoglobulin on mature B cells by inducible gene targeting results in rapid cell death. Cell. 1997; 90:1073–1083. [PubMed: 9323135]

35. Rajewsky K. Clonal selection and learning in the antibody system. Nature. 1996; 381:751–758. [PubMed: 8657279]
36. Srinivasan L, et al. PI3 kinase signals BCR-dependent mature B cell survival. Cell. 2009; 139:573–586. [PubMed: 19879843]
37. Shaner NC, et al. A bright monomeric green fluorescent protein derived from Branchiostoma lanceolatum. Nat Methods. 2013; 10:407–409. [PubMed: 23524392]
38. Tyas L, Brophy VA, Pope A, Rivett AJ, Tavare JM. Rapid caspase-3 activation during apoptosis revealed using fluorescence-resonance energy transfer. EMBO Rep. 2000; 1:266–270. [PubMed: 11256610]
39. Lam AJ, et al. Improving FRET dynamic range with bright green and red fluorescent proteins. Nat Methods. 2012; 9:1005–1012. [PubMed: 22961245]
40. Robbiani DF, et al. AID produces DNA double-strand breaks in non-Ig genes and mature B cell lymphomas with reciprocal chromosome translocations. Mol Cell. 2009; 36:631–641. [PubMed: 19941823]
41. Robbiani DF, Colon K, Affer M, Chesi M, Bergsagel PL. Maintained rules of development in a mouse B-cell tumor. Leukemia. 2005; 19:1278–1280. [PubMed: 15843816]
42. Thai TH, et al. Regulation of the germinal center response by microRNA-155. Science. 2007; 316:604–608. [PubMed: 17463289]
43. Warming S, Costantino N, Court DL, Jenkins NA, Copeland NG. Simple and highly efficient BAC recombineering using galK selection. Nucleic Acids Res. 2005; 33:e36. [PubMed: 15731329]
44. Guo M, et al. A monoclonal antibody to the DEC-205 endocytosis receptor on human dendritic cells. Hum Immunol. 2000; 61:729–738. [PubMed: 10980384]
45. Shih TA, Roederer M, Nussenzweig MC. Role of antigen receptor affinity in T cell-independent antibody responses in vivo. Nat Immunol. 2002; 3:399–406. [PubMed: 11896394]
46. Meredith MM, et al. Expression of the zinc finger transcription factor zDC (Zbtb46, Btbd4) defines the classical dendritic cell lineage. J Exp Med. 2012; 209:1153–1165. [PubMed: 22615130]
47. Robbiani DF, et al. AID is required for the chromosomal breaks in c-myc that lead to c-myc/IgH translocations. Cell. 2008; 135:1028–1038. [PubMed: 19070574]
48. von Boehmer L, et al. Sequencing and cloning of antigen-specific antibodies from mouse memory B cells. Nat Protoc. 2016; 11:1908–1923. [PubMed: 27658009]
49. Dosenovic P, et al. Immunization for HIV-1 Broadly Neutralizing Antibodies in Human Ig Knockin Mice. Cell. 2015; 161:1505–1515. [PubMed: 26091035]
50. Allen D, Simon T, Sablitzky F, Rajewsky K, Cumano A. Antibody engineering for the analysis of affinity maturation of an anti-hapten response. EMBO J. 1988; 7:1995–2001. [PubMed: 3138111]
51. Cumano A, Rajewsky K. Clonal recruitment and somatic mutation in the generation of immunological memory to the hapten NP. EMBO J. 1986; 5:2459–2468. [PubMed: 2430792]
52. Wardemann H, et al. Predominant autoantibody production by early human B cell precursors. Science. 2003; 301:1374–1377. [PubMed: 12920303]

One Sentence Summary

The mechanisms regulating cell death in the germinal center are microanatomically segregated.

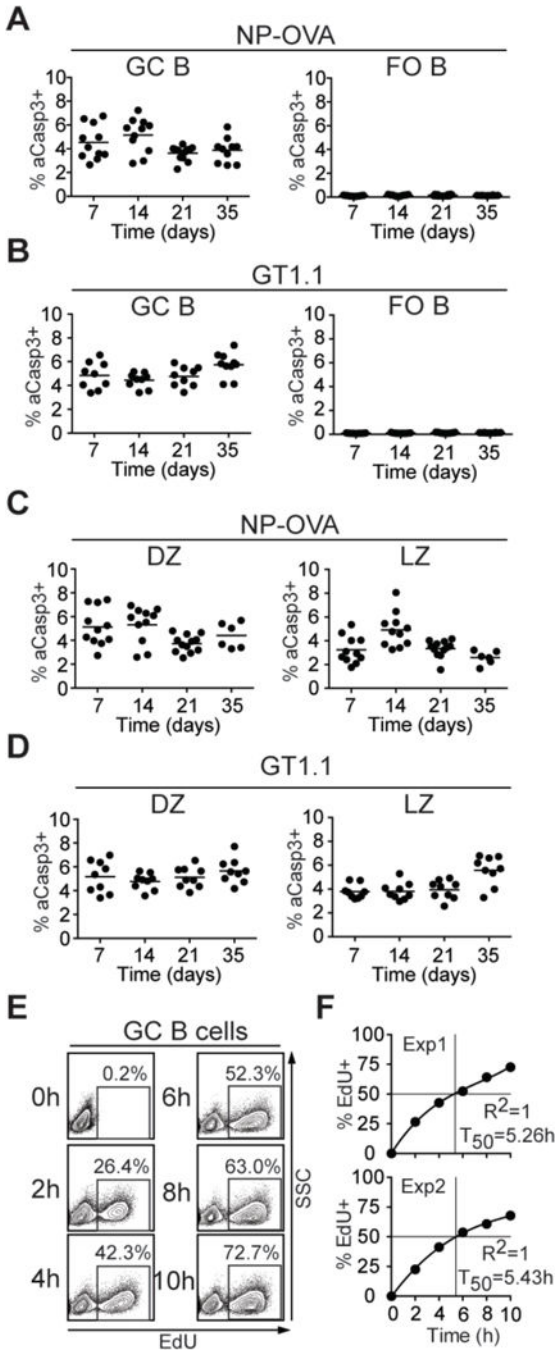

Fig. 1. Quantitation of cell death in GC B cells

(**A-D**) C57BL/6J mice were immunized subcutaneously with NP-OVA or GT1.1 precipitated in alum and analyzed after 7, 14, 21, and 35 d. Percentages of aCasp3^{+} GC B cells and FO B cells (left and right, respectively) after (**A**) NP-OVA or (**B**) GT1.1 immunization. Percentages of aCasp3^{+} cells in CXCR4^{hi}CD86^{lo} (DZ, left) and CXCR4^{lo}CD86^{hi} (LZ, right) after (**C**) NP-OVA or (**D**) GT1.1 immunization. In **A-D**, each dot represents one mouse. (**E, F**) EdU incorporation into Peyer's patch GC B cells measured by flow cytometry at the indicated time points after EdU administration every 2 h. (**E**) Representative flow cytometry

plots show EdU and side scatter (SSC). (**F**) Plots show fraction of EdU^+ GC B cells vs. time. T_{50} represents the interpolated time (cubic fit) where 50% of GC B cells incorporated EdU. Data are from at least two independent experiments each involving 2-5 mice for every time point.

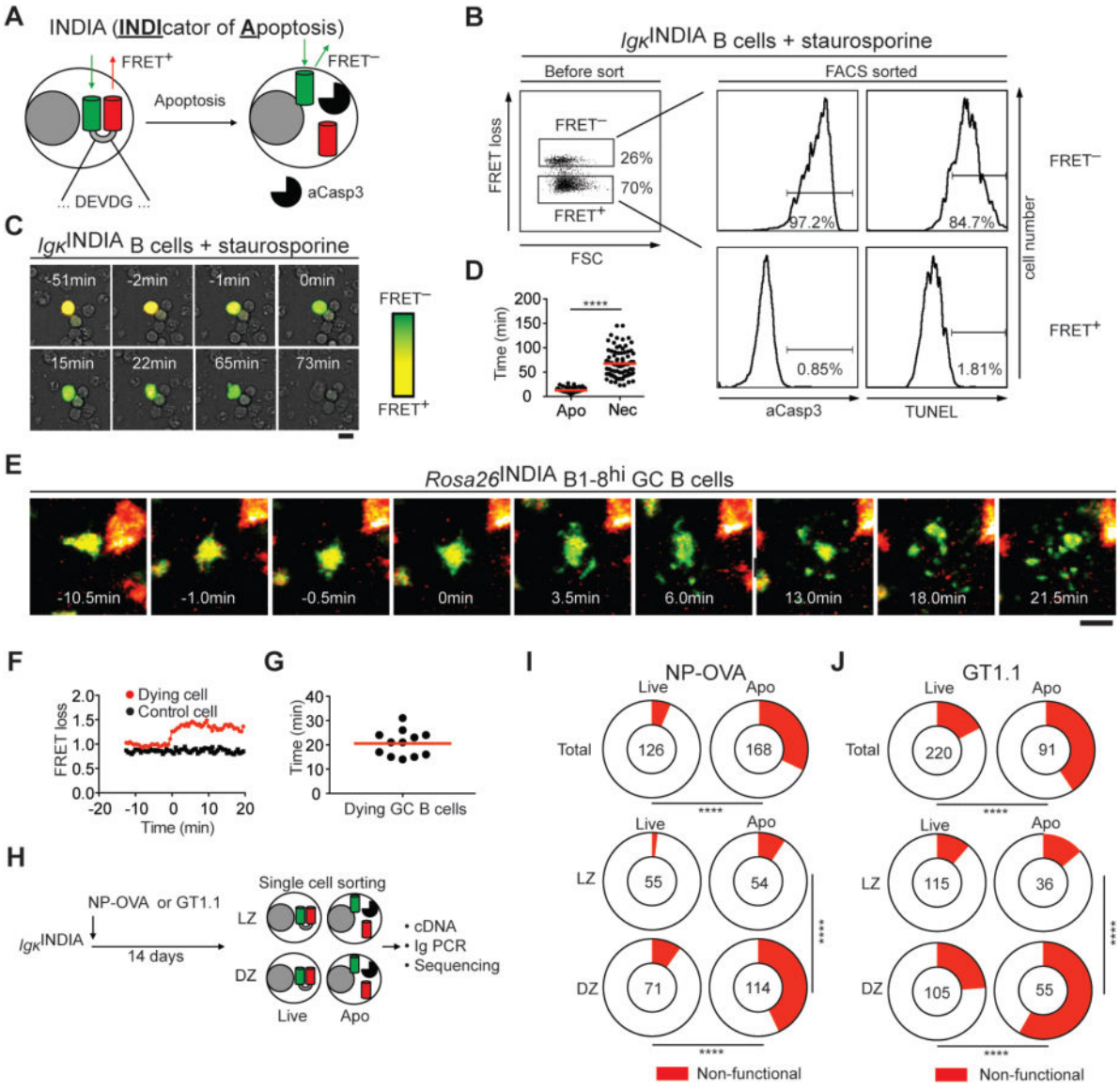

Fig. 2. Cell death dynamics and selection against BCR loss

(**A**) Schematic representation of the apoptosis indicator. (**B**) Flow cytometry of LPS/IL-4-activated *Igκ*^{INDIA} B cells incubated with staurosporine for 3 h. Dot plot shows forward scatter (FSC) and FRET loss of mRuby2^{+} cells. Histograms show aCasp3 or TUNEL staining on purified FRET^{+} and FRET$^{−}$ cells. (**C**) Representative images of LPS/IL-4-activated *Igκ*^{INDIA} B cells showing FRET loss as increased green fluorescence over time after addition of staurosporine (scale bar: 10 μm). (**D**) Time from initiation of FRET loss (synchronized to 0 min) to signs of apoptosis (Apo) or necrosis (Nec; Apo: n = 70 cells; Nec: n = 82 cells; **** $p < 0.0001$, two-tailed Mann-Whitney *U* test). (**E-G**) Intravital imaging of B1-8^{hi} *Rosa26*^{INDIA} GC B cells in lymph nodes of NP-OVA immunized mice. (**E**) Collapsed Z-stacks of 75-μm depth showing FRET loss and disintegration of a GC B-cell over time. (**F**) FRET loss ratios tracked over time (red, the dying cell in (**E**); black, a live GC B-cell in the same imaging volume). (**G**) Time from FRET loss to GC B-cell

fragmentation. (**H-J**) Paired *IgH/Igλ* or *IgH/*Ig*κ* sequences from single *Igκ*^{INDIA} live and apoptotic GC LZ and DZ B cells purified from NP-OVA- or GT1.1-immunized mice. (**H**) Schematic representation of the experiment. (**I, J**) Pie charts show the fraction of non-functional BCRs (red) in live and apoptotic GC B cells (top) or in LZ and DZ (bottom) after (**I**) NP-OVA and (**J**) GT1.1 immunization. Number in the center indicates the number of *Ig* pairs analyzed. Data are from at least two independent experiments in all cases. **** $p < 0.0001$; Fisher's exact test.

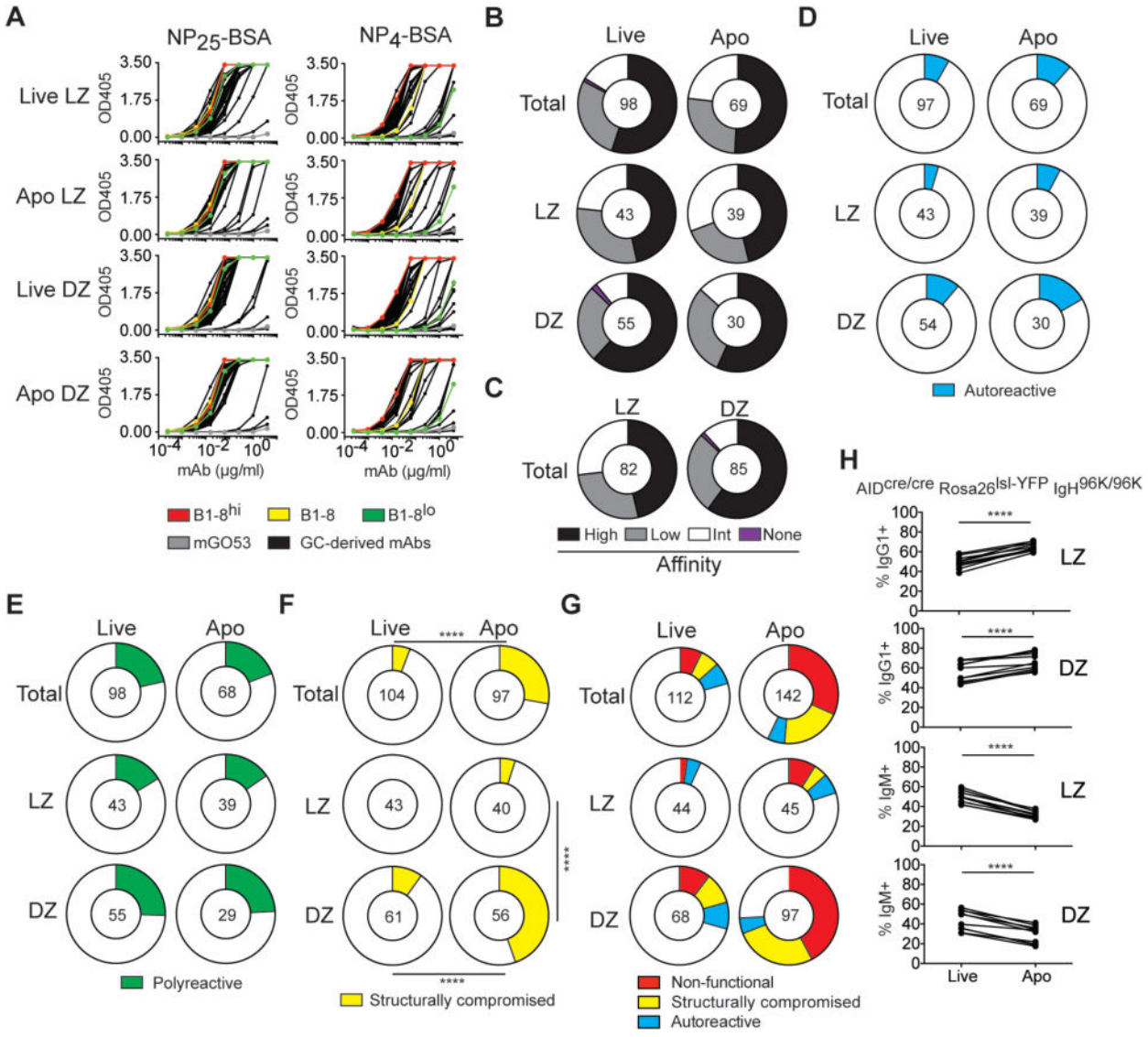

Fig. 3. Binding properties of GC-derived $IgH_{V1\text{-}72}$ $Ig\lambda$ antibodies

(**A**) ELISAs show monoclonal antibody binding to NP_{25}-BSA (left) or NP_4-BSA (right); NP-specific control antibodies (B1-8^{hi}, high-affinity, red; B1-8 germline, intermediate-affinity, yellow; B1-8^{lo}, low-affinity, green) and mGO53 (negative control, grey) are included. (**B**) Pie charts show the percentage of high-, low-, and intermediate-affinity antibodies in each GC compartment (NP_4/NP_{25} ratio = 1, black; < B1-8 germline, grey; > B1-8 germline < 1; white), or no NP binding (magenta). (**C**) Same as (**B**) but for all LZ and DZ cells irrespective of cell death. (**D**) Percentage of antibodies binding to self-antigens in HEp2 ELISA (cyan). (**E**) Percentage of polyreactive antibodies (green). (**F**) Percentage of structurally compromised antibodies that cannot be secreted by transfected HEK293-6E cells (yellow). (**G**) Summary of negative selection in GCs. Percentage of non-functional BCRs (see Fig. 2I), structurally compromised BCRs (yellow slice), and autoreactive BCRs (cyan slice) in each GC B-cell compartment. (**B-G**) The number in the center of the pie charts represents the number of antibodies tested. (**H**) Graphs show the fraction of $IgG1^+$

and IgM^{+} live and apoptotic Peyer's patch DZ and LZ GC B cells in *AID*$^{Cre/Cre}$*Rosa26*$^{lsl\text{-}YFP}$*IgH*$^{96K/96K}$ mice as determined by aCasp3 staining. Results are combined from two independent experiments each involving 3-5mice. **** $p < 0.0001$; paired Student's *t*-test.

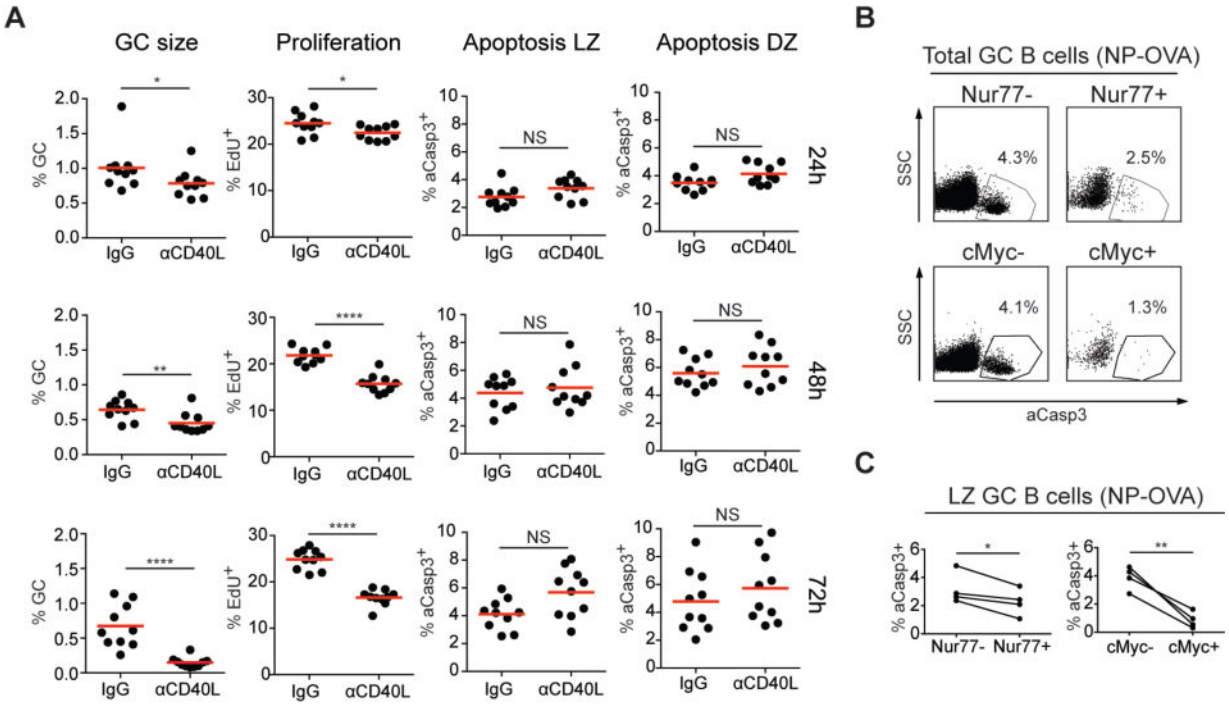

Fig. 4. Apoptosis in the GC LZ

(**A**) Graphs show the fraction of GC B cells among CD19$^+$ B cells (left column), fraction of EdU$^+$ GC B cells (second column) and fraction of aCasp3$^+$ cells in GC LZ and DZ (right columns) in the draining lymph nodes of C57BL/6J mice 14 d after NP-OVA immunization. Hamster IgG or α-CD40L was injected 24 h, 48 h or 72 h before analysis. Results are combined from two independent experiments each with five mice per condition. * p = 0.037 (24 h, GC size), * p=0.0215 (24 h, proliferation), ** p = 0.0048, **** p < 0.0001, NS p > 0.05 (not statistically significant); two-tailed Mann-Whitney *U* test. (**B, C**) Analysis of apoptosis in GC B cells in *Nur77*-GFP or *Myc*-GFP mice 14 d after immunization with NP-OVA. (**B**) Representative flow cytometry plots show the frequency of aCasp3$^+$ cells in *Nur77*-GFP$^-$ and *Nur77*-GFP$^+$ (top) and in *Myc*-GFP$^-$ and *Myc*-GFP$^+$ GC B cells (bottom). (**C**) The frequency of aCasp3$^+$ cells in *Nur77*-GFP$^-$ and *Nur77*-GFP$^+$ (left graph), or *Myc*-GFP$^-$ and Myc-GFP$^+$ LZ GC B cells (right graph). (**B, C**) Two to three independent experiments each involving 3-6 *Nur77*-GFP or *Myc*-GFP mice with three mice pooled per data set. *Nur77*-GFP, * p = 0.0355; *Myc*-GFP, ** p = 0.006; paired Student's *t*-test.